small methods
www.small-methods.com

Low-Power, Multi-Transduction Nanosensor Array for Accurate Sensing of Flammable and Toxic Gases

Dionisio V. Del Orbe Henriquez, Mingu Kang, Incheol Cho, Jungrak Choi, Jaeho Park, Osman Gul, Junseong Ahn, Dae-Sik Lee, and Inkyu Park**

Toxic and flammable gases pose a major safety risk in industrial settings; thus, their portable sensing is desired, which requires sensors with fast response, low-power consumption, and accurate detection. Herein, a low-power, multi-transduction array is presented for the accurate sensing of flammable and toxic gases. Specifically, four different sensors are integrated on a micro-electro-mechanical-systems platform consisting of bridge-type microheaters. To produce distinct fingerprints for enhanced selectivity, the four sensors operate based on two different transduction mechanisms: chemiresistive and calorimetric sensing. Local, in situ synthesis routes are used to integrate nanostructured materials (ZnO, CuO, and Pt Black) for the sensors on the microheaters. The transient responses of the four sensors are fed to a convolutional neural network for real-time classification and regression of five different gases (H_2, NO_2, C_2H_6O, CO, and NH_3). An overall classification accuracy of 97.95%, an average regression error of 14%, and a power consumption of 7 mW per device are obtained. The combination of a versatile low-power platform, local integration of nanomaterials, different transduction mechanisms, and a real-time machine learning strategy presented herein helps advance the constant need to simultaneously achieve fast, low-power, and selective gas sensing of flammable and toxic gases.

1. Introduction

Many important but hazardous gases in the industry are toxic and/or flammable. To ensure the safety of workers and properties, accurate and portable gas sensing is desired. Accordingly, various research approaches have been developed to improve the performance characteristics of gas sensors. Specifically, nanomaterials have been synthesized to achieve high sensitivity and high selectivity;[1–4] also, micro-electro-mechanical-systems (MEMS) platforms have been designed for low-power consumption and fast response speeds;[5] and batch fabrication processes have been used to reduce the cost.[6,7] However, it is challenging to achieve all or most of the desired performance parameters simultaneously using a single sensor, largely due to the cross-sensitivity of a sensor.[1] Thus, research has come to use arrays of different gas sensors with a focus on enhancing discrimination performance while attaining a low-power consumption, key metrics for an array.

Recently developed chemiresistive-type gas sensors are made of different metal oxide nanomaterials and/or doping with metal nanoparticles on integrated heaters.[3,4,6,8–11] They are attractive for gas sensing arrays because each sensor's selectivity can be tuned and they can be miniaturized for low-power consumption.[3,4,6,9–11] However, although good discrimination performances have been shown with chemiresistive arrays through rational designs and statistical analyses,[8,11] the sensors have broad selectivity, that is, they respond to many gases; this potentially limits the discrimination performance because multiple sensors are contributing similar information about a gas.[12] Combining different transduction mechanisms, besides chemiresistive type, is a way to help improve this issue.

Multi-transduction arrays can show better discrimination performance[13–15] and require less number of constituent sensors[14,15] than single transduction arrays; this is due to their orthogonal responses to the target gases in the chemical feature space.[12,16] For example, in previous work[15] for the detection of contraband food, 19 sensors (comprising 3 different transduction mechanisms) were combined in different sub-arrays to compare their performance; the results show that the best subset-array of 2 sensors (from two different transduction mechanisms) showed better performance than any single-transduction combination. In general, the various types of gas sensors contained in arrays use different physicochemical properties of the target analytes, including, combustibility (catalytic combustion sensors),[17,18] thermal conductivity,[17,19] mass (gravimetric),[20–22] electrochemical properties (electrochemical

D. V. Del Orbe Henriquez, M. Kang, I. Cho, J. Choi, J. Park, O. Gul, J. Ahn, I. Park
Department of Mechanical Engineering
Korea Advanced Institute of Science and Technology
291, Daehak-ro, Yuseong-gu, Daejeon 34141, Republic of Korea
E-mail: inkyu@kaist.ac.kr

D. V. Del Orbe Henriquez, D.-S. Lee
Welfare & Medical ICT Research Department
Electronics and Telecommunications Research Institute
218, Gajeong-ro, Yuseong-gu, Daejeon 34129, Republic of Korea
E-mail: dslee@etri.re.kr

D. V. Del Orbe Henriquez
College of Engineering
Universidad APEC (UNAPEC)
Santo Domingo 10100, Dominican Republic

The ORCID identification number(s) for the author(s) of this article can be found under https://doi.org/10.1002/smtd.202201352.

DOI: 10.1002/smtd.202201352

© 2023 Wiley-VCH GmbH

Check for updates
23669608, 2023, 3, Downloaded from https://onlinelibrary.wiley.com/doi/10.1002/smtd.202201352 by Korea Advanced Institute Of, Wiley Online Library on [20/03/2023]. See the Terms and Conditions (https://onlinelibrary.wiley.com/terms-and-conditions) on Wiley Online Library for rules of use; OA articles are governed by the applicable Creative Commons License

sensors),[23] light modulation (optical sensors),[16,24] etc. Which type of sensor to combine in a multi-transduction array depends on the specific application, selectivity ranges of the constituent sensors,[12] and compatibility of materials and processes. Interestingly, the performance of multi-transduction arrays has been reported to increase if we combine sensors with different selectivity to the different gases (narrow, medium, and broad selectivity); here, narrow selectivity indicates a sensor is selective (responsive) to very few gases while broad selectivity indicates the responsiveness of a sensor to many gases.[12,25] In this regard, chemiresistive-type sensors (N-type and P-type) and calorimetric-type sensors (thermal conductivity and catalytic combustion) are appropriate candidates for multi-transduction sensor arrays for low-power, high-accuracy sensing of flammable and toxic gases. These sensors show various ranges of selectivity, for example, chemiresistive sensors have wider sensitive ranges than thermal conductivity sensors; additionally, they have the ability to be miniaturized[4,17] and require similar circuity, that is, they monitor resistance changes. Another complementary advantage of the chemiresistive and calorimetric sensors is that metal oxides perform better at lower gas concentrations (in parts per million, ppm) whereas calorimetric sensors perform better at higher concentrations (up to a few percent).[26] However, finding compatible fabrication and integration methods for the different sensing materials/catalysts in a miniaturized chip is one of the main challenges in fabricating this type of multi-transduction array. Additionally, to simultaneously achieve low-power consumption, fast response, high sensitivity, various sensitivity characteristics of the constituent sensors, and accurate sensing, that is, comparable to modern-day gas sensors and arrays, it is imperative to apply a combination of techniques such as MEMS technology, local integration methods, nanomaterials, and machine learning.

Herein, we present a multi-transduction gas-sensing array composed of four sensors, two chemiresistive devices (N-type and P-type), and two calorimetric devices (catalytic and thermal conductivity) for accurate and low-power detection of five flammable/toxic gases in real-time (with the aid of a machine learning algorithm). Nanostructured metal oxides for the chemiresistive devices (and a noble metal catalyst for the catalytic sensor) are integrated on a MEMS platform via successive, compatible localized synthesis methods (local hydrothermal synthesis[4,7] and local electrodeposition).[17] This fabrication strategy allows for the integration of the nanomaterials in a very small area and helps to simultaneously achieve low-power consumption, fast response, and high sensitivity. Compared to other miniaturized chemiresistive and multi-transduction arrays in previous studies, the device fabricated in this work has the scalability of the fabrication process and also can be driven with very low power consumption.[10,6,21,27] The constituent sensors in the array were selected to display various sensitivity characteristics depending on the properties of the target gases, which contribute to accurate gas sensing. We justified the selected combination of the constituent sensors by using principal component analysis (PCA). As non-supervised learning techniques do not allow for real-time detection, we have implemented a machine learning technique based on convolutional neural networks (CNNs) and a transient sliding window for real-time classification and quantification (regression) of the different gases,[6] achieving gas identification in real-time even using the response data at the specific concentration not used for training the network.

2. Results and Discussion

2.1. Description of the Fabricated Array and Sensing Strategy

Figure 1 shows an overview of the work reported herein: a schematic representation of the multi-transduction gas sensing array (Figure 1a), optical microscope images of the fabricated array consisting of the 4 sensors (Figure 1b), scanning electron microscope images of the locally-synthesized nanomaterials (Figure 1c), and the gas sensing strategy utilized for the accurate sensing of flammable and toxic gases (Figure 1d). As shown in Figure 1a,b, all sensors consist of identical bridge-type microheaters with small active areas of 9 μm × 110 μm (per individual sensor) for fast responses and low-power operations (7 mW per device). For the calorimetric sensors, the resistances of the microheaters are recorded as they change in response to a target gas, while in the case of chemiresistive sensors (CuO nanosheets for the P-type sensor and ZnO nanowires for the N-type), the resistances of the nanomaterials are recorded as they change in response to a target gas; thus, for the calorimetric devices, the microheaters also act as resistive temperature detectors (RTDs). The calorimetric devices have Au electrodeposition electrodes on top of the microheater, which allow the electrodeposition of the catalyst (nanostructured Pt Black) for the catalytic combustion sensor; the thermal conductivity sensor does not have any nanomaterial integrated and the electrode is fabricated to match the thermal characteristics of the catalytic combustion sensor (this helps distinguish when an atmosphere is flammable as explain hereinafter). Both calorimetric sensors react to thermal conductivity changes in an environment but the catalytic combustion sensor also experiences an increase in resistance if a flammable gas is combusted on the surface of the catalyst (indicating the presence of a flammable gas/atmosphere). On the other hand, the chemiresistive devices have pairs of Au electrodes (with a 3 μm gap) to sense the resistance changes of the nanomaterials above them. The integration of the sensing layers (CuO and ZnO) and nanocatalysts (Pt Black) on these small areas of the microheaters is achieved by the use of successive, compatible local synthesis processes, that is, local hydrothermal synthesis[4,7] for CuO and ZnO and local electrodeposition for Pt Black.[17] Using the transient response of each constituent sensor, Figure 1d shows an overview of the machine-learning strategy used for real-time classification and regression. Specifically, a 5-second-sliding window for each of the responses is used to build a tensor that gets passed to a CNN architecture, ultimately outputting the gas class (gas type) and regression values (concentration) in real time.

Based on their flammability limits and levels of toxicity, the hazardous gases studied herein (H_2, NO_2, C_2H_6O, CO, and NH_3) have different risk-relevant concentrations as presented in Table S1 (Supporting Information); here, we test concentrations for each gas below its flammability range or permissible exposure limit, whichever of the two is lower for a particular

© 2023 Wiley-VCH GmbH

23669608, 2023, 3, Downloaded from https://onlinelibrary.wiley.com/doi/10.1002/smtd.202201352 by Korea Advanced Institute Of, Wiley Online Library on [20/03/2023]. See the Terms and Conditions (https://onlinelibrary.wiley.com/terms-and-conditions) on Wiley Online Library for rules of use; OA articles are governed by the applicable Creative Commons License

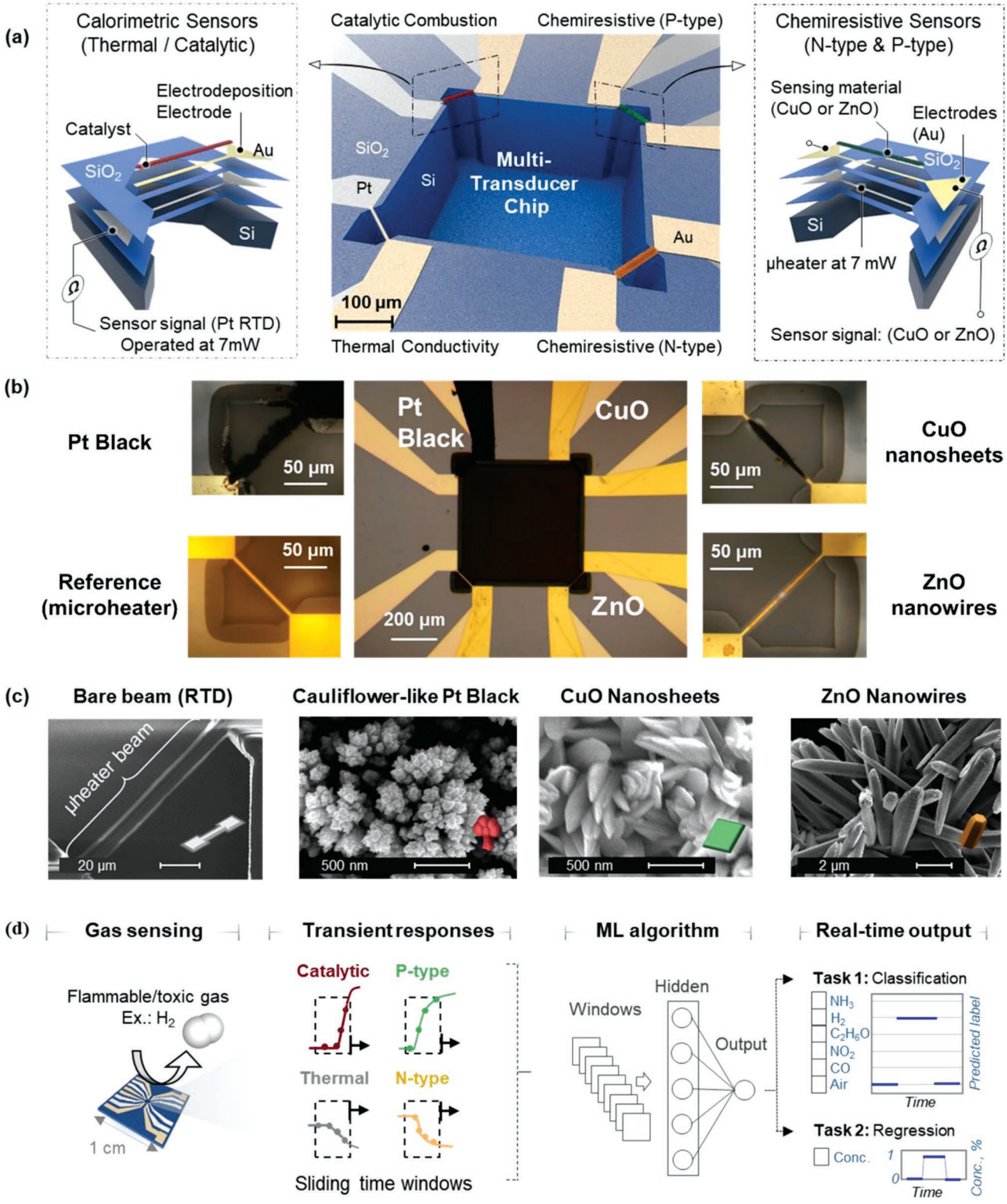


Figure 1. Overview of the multi-transduction gas sensor array for real-time gas sensing. a) Schematic representation of the constituent sensors in the array, including exploded views of the layers (sides). b) Optical microscope images of the fabricated array with all sensing materials synthesized. c) Scanning Electron Microscope images of the fabricated nanomaterials on their respective microheaters; the thermal conductivity sensor does not carry any nanomaterial and the bare microheater beam is shown here. d) Overview of the machine learning strategy, whereby transient responses are processed for real-time classification and regression.

© 2023 Wiley-VCH GmbH

23669608, 2023, 3, Downloaded from https://onlinelibrary.wiley.com/doi/10.1002/smtd.202201352 by Korea Advanced Institute Of, Wiley Online Library on [20/03/2023]. See the Terms and Conditions (https://onlinelibrary.wiley.com/terms-and-conditions) on Wiley Online Library for rules of use; OA articles are governed by the applicable Creative Commons License

gas. Figure S1 (Supporting Information) shows the constituent sensors of the fabricated array and their cross-sensitivity to each of the tested gases. The sensors in the array were fabricated to have these various ranges of selectivity for the different gases because having different selectivity ranges in an array helps to achieve better discrimination performance.[12,25]

2.2. Device Fabrication: MEMS Platform and Localized, In Situ Synthesis of Nanomaterials

Each nanomaterial is synthesized locally on the low-power MEMS platform (**Figure 2**a). To fabricate the multi-transduction arrays, not only the calorimetric-type sensors but also the chemiresistive-type sensors should be integrated into the device. The local syntheses (integration techniques) of the nanomaterials follow four basic sequential steps as shown in Figure 2b–e. The first step consists of sputtering SnO_2 seeds on the entire chip. This plants the seeds for the subsequent growth of the metal oxides (CuO and ZnO) in steps 3 and 4. Before growing the metal oxides, the Pt nanostructures are grown in situ via electrodeposition with 0.1% platinic acid (with 0.005% lead acetate); this is a modified version of our previous work to avoid etching of the sputtered seeds.[17] The Pt in the platinic acid is generally reduced from platinum (IV) to platinum (II) and then to platinum (0) or directly from platinum (IV) to platinum (0).[28] Through an electric field, the metal complexes $Pt^{IV}Cl_6^{2-}$ or $Pt^{II}Cl_4^{2-}$ approach the cathode, and the reduction of the Pt is conducted through an ad-atom mechanism.[29] The synthesized Pt nanostructures by electrodeposition have a pseudo-porous structure with interconnected sphere-like protrusions of ≈40–110 nm.[17] Since the pseudo-porous structure facilitates the target gases to diffuse easily and provides high thermal conductivity to the embedded RTD easily, this structure is advantageous for gas sensing. For the chemiresistive type sensors, ZnO and CuO were used in this work, and these semiconducting materials can react with the gases at high-temperature conditions (above 150 °C). To generate the high-temperature conditions (≈250 °C), the metal oxides were integrated into the microheaters. Their sensing mechanism is based on their resistance change in the presence of a target gas that is explained by the removal or coverage of oxygen ions (O^- and O^{2-}) from the surface of the metal oxide.[4] Due to the sensing mechanism of the chemiresistive type sensors, it is important to increase the surface-to-volume ratio of the sensing materials for improved sensing performance. Therefore, the local hydrothermal synthesis method was selected to locally integrate the metal oxide sensing materials with a large surface area on the bridge-type microheater. In steps 3 and 4, ZnO nanowires and CuO nanosheets are grown, respectively. By putting a Polydimethylsiloxane well on top of the chip, we can deposit a small volume of the ZnO or CuO precursor solution

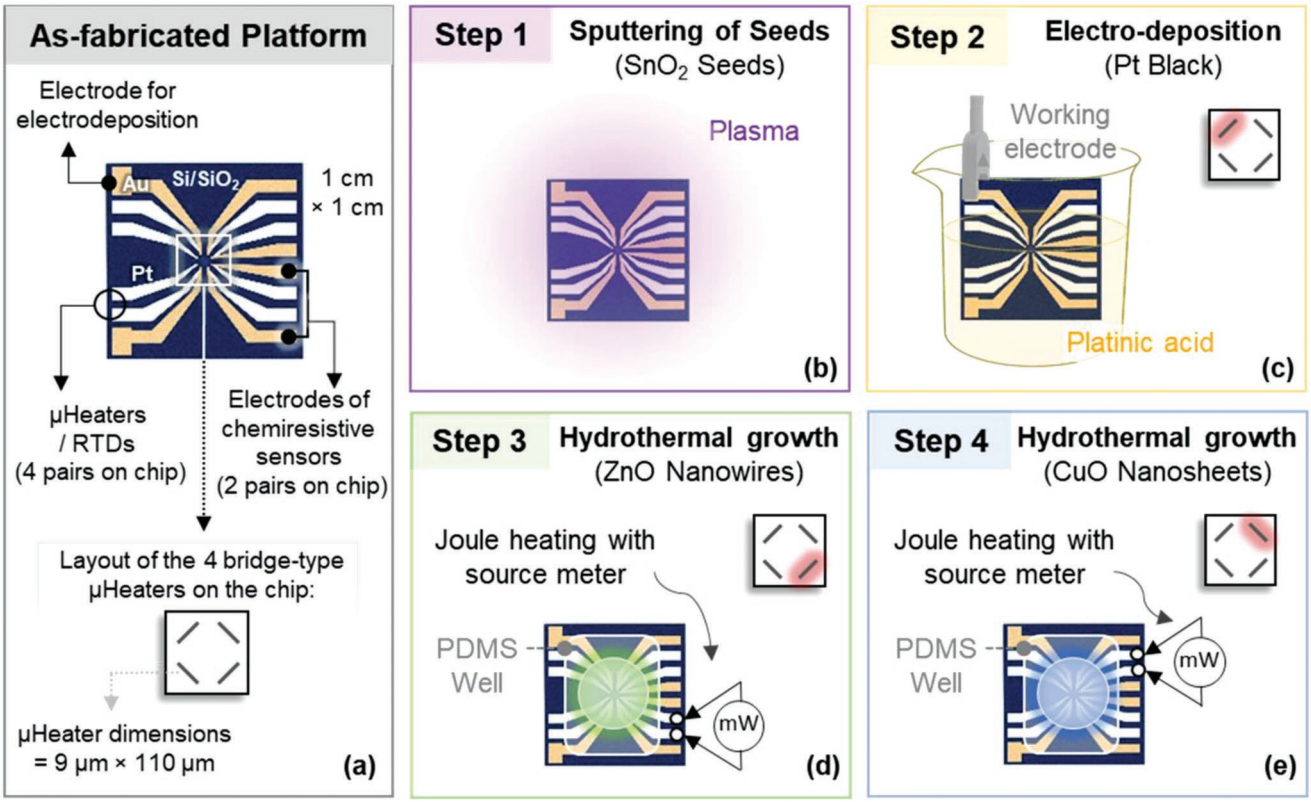


Figure 2. Overview of the fabrication process (integration of nanomaterials). a) top view of the chip. b) Step 1 consists of depositing the SnO_2 seed layer for eventual hydrothermal growth. c) The nanostructured Pt Black is synthesized via electrodeposition (the solution does not affect the seed layer). d) Local hydrothermal growth of ZnO nanowires using joule heating. e) Local hydrothermal growth of CuO nanosheets using joule heating. In steps 2–4, rinsing in acetone and ethanol is performed between steps and at the end.

© 2023 Wiley-VCH GmbH

23669608, 2023, 3, Downloaded from https://onlinelibrary.wiley.com/doi/10.1002/smtd.202201352 by Korea Advanced Institute Of, Wiley Online Library on [20/03/2023]. See the Terms and Conditions (https://onlinelibrary.wiley.com/terms-and-conditions) on Wiley Online Library for rules of use; OA articles are governed by the applicable Creative Commons License

to later grow the nanostructures of each material in situ when Joule heating is applied to the submerged microheater. When an electrical voltage was applied to the microheater in the ZnO or CuO precursor solution, convective mass transfer of precursor solution was generated by a localized temperature rise via the Joule heating.[4,30] The nanostructured ZnO and CuO could be integrated into the microheater by endothermal reaction of precursor chemicals, and the fresh precursor could be supplied to the microheater by the convective mass transfer.[4] Finally, the ZnO nanowires and CuO nanosheets with large surface-to-volume ratios were successfully integrated into the microheater. Table S2 (Supporting Information) lists the metal salts and other parameters for these hydrothermal growth processes. Finally, by using the developed local integration techniques, chemiresistive-type and calorimetric-type sensors could be used in the same device, unlike the previous works.[4,7,17,30] The crystalline characteristics of the Pt black are well described in our previous work,[17] and through the X-ray diffraction analysis, it was confirmed that highly crystalline structures of ZnO nanowires and CuO nanosheets were well synthesized by the hydrothermal method (Figure S2, Supporting Information).

It is noteworthy to mention that, during the fabrication, the order for the integration of each nanomaterial is important. The sequence for the integration of the nanomaterials (as in Figure 2) was established by studying the compatibility of the different nanostructures to the different precursors; for example, Table S3 (Supporting Information) shows that it is important to sputter the SnO_2 nanoparticles before the electrodeposition of the Pt black because the sputtered particles decrease the performance of the catalytic sensor if done after synthesis of the Pt catalyst. Similarly, the CuO precursor can etch away the ZnO nanowires if they are immersed for a long time. Thus, the sequence in Figure 2 and the parameters in Table S2 (Supporting Information) ensure compatibility in the fabrication of the array through the use of these local integration techniques for small-area integration of metal oxides and catalyst material.

2.3. Gas Sensor Responses and Operating Temperature

Figure 3a shows the transient responses of all four sensors tested simultaneously to the five different toxic/flammable gases. As summarized in Figure 3b, the magnitude and direction of the responses for all the sensors are different for most gases, constituting a unique "fingerprint" for each gas, favorable for gas identification. The trend and magnitude of each response correspond to how each sensor reacts to a particular gas. First, in the case of the catalytic combustion sensor, the H_2 gas is locally combusted by the Pt-black catalyst.[17] This local combustion increases the temperature of the microheater, and thus the resistance of the underlying heater increases. On the other hand, in the case of a thermal conductivity sensor, local combustion cannot occur because there is no catalyst for combustion. Instead, since H_2 gas has higher thermal conductivity compared to the air, H_2 gas causes a cooling effect on the thermal conductivity sensor. As a result, the resistance of the conductivity sensor decreases. In the case of C_2H_6O and NH_3 gases, the resistance of both the catalytic combustion and thermal conductivity sensor decrease because they do not cause the catalytic combustion but have higher thermal conductivity than the air. On the other hand, since NO_2 and CO gases have similar thermal conductivities to air at the operating temperature of the sensors, it is hard to see the response of the catalytic combustion and thermal conductivity sensor to those gases. For the chemiresistive type sensors, the oxygen ions are chemisorbed on the surface of the metal oxide in the high-temperature conditions above 150 °C and produce different effects on N-type and P-type metal oxides.[4,31] For the N-type metal oxide, the adsorbed oxygens pull electrons from the metal oxide, which generates the electron depletion layer. On the other hand, for the P-type metal oxide, a hole accumulation layer is generated by the adsorbed oxygens. Therefore, under reducing gas conditions, the adsorbed oxygen on the N-type metal oxide reacts with the reducing gases, and in this process, electrons are supplied to the N-type metal oxide, which reduces the resistance of the N-type metal oxide. In contrast, under oxidizing gas conditions, the resistance of the N-type metal oxide increases because the electron depletion layer increases due to the deprivation of the electron in the reaction process. The opposite phenomenon occurs in the resistance change of the P-type metal oxide since the major carrier of the P-type metal oxide is the hole. In this work, for the chemiresistive type sensors, ZnO (N-type) and CuO (P-type) were used, and they were integrated into the microheaters to generate the high-temperature condition (≈250 °C). Since the ZnO is N-type metal oxide, the responses of the ZnO sensor were smaller than 1 to the reducing gases (H_2, C_2H_6O. CO, and NH_3) and larger than 1 to the oxidizing gas (NO_2). On the other hand, the responses of the CuO sensor showed the opposite tendency because CuO is a P-type metal oxide. This property-specific response in each sensor is beneficial for gas sensing as we aim to combine sensors that respond differently to each gas in the chemical feature space.[12]

After performing a temperature calibration of the chip (shown in Figure S3, Supporting Information), the surface temperature of the microheaters at 7 mW is estimated to be 252 °C. This operating power was chosen because it yields the maximum sensitivity for all constituent sensors with good reliability for the platform.[4,17] Furthermore, from the calibration, it was also found that for the calorimetric sensors, the temperature change per resistance change is 21.17 °C Ω^{-1}, for example, during the exposure of 1.6% H_2, the temperature increases by ≈12 °C for the catalytic combustion sensor and it decreases by ≈2 °C for the thermal conductivity sensor.

2.4. 2.4. Analysis of Possible Sensor Combinations and Discrimination Performance

As shown in **Figure 4**a, we performed PCA with all possible combinations of the four constituent sensors to evaluate their discrimination performance with cluster analysis; the subarrays included combinations of 2 sensors, 3 sensors, and 4 sensors. When the response data of only two types of sensors were used, the cluster analysis should be conducted in the 2D plane. Therefore, in this work, the PCA for reduction of dimension was conducted even when response data of three and four

© 2023 Wiley-VCH GmbH

23669608, 2023, 3, Downloaded from https://onlinelibrary.wiley.com/doi/10.1002/smtd.202201352 by Korea Advanced Institute Of, Wiley Online Library on [20/03/2023]. See the Terms and Conditions (https://onlinelibrary.wiley.com/terms-and-conditions) on Wiley Online Library for rules of use; OA articles are governed by the applicable Creative Commons License

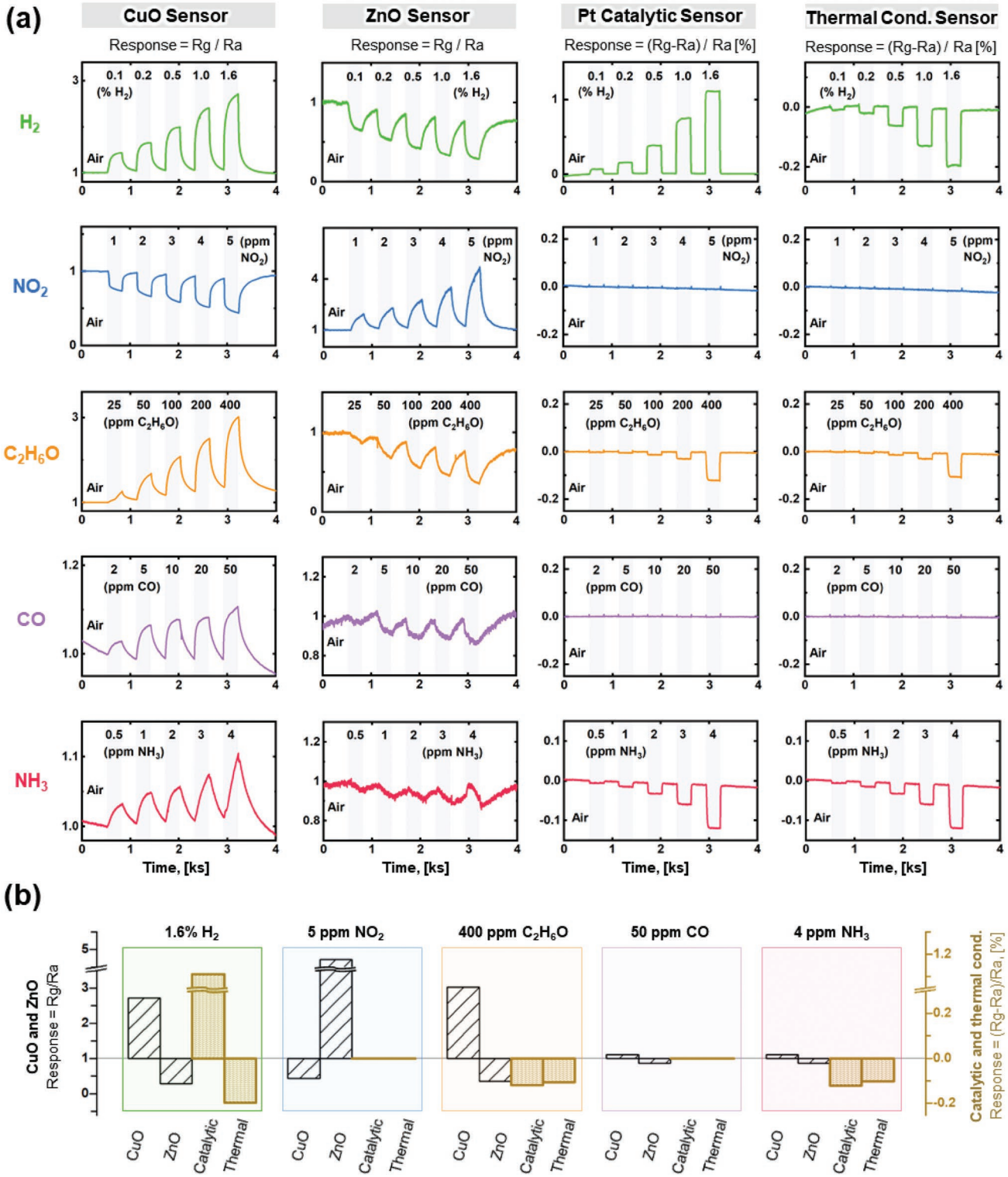


Figure 3. a). Dynamic responses of the chemiresistive sensors (CuO and ZnO) and the calorimetric sensors (catalytic combustion and thermal conductivity) to the exposure of risk-relevant concentrations of H_2, NO_2, C_2H_6O, CO, and NH_3. b) Summary of the responses of the four sensors shown in part (a); the chemiresistive sensors have the same definition for their response (left axis), as do the calorimetric sensors (right axis).

types of sensors were used to compare the analysis results in the same criteria. Given the limited number of sensors and target gases, it is difficult to draw broad conclusions; however, several inferences can be drawn from this work, consistent with similar analyses done in previous literature.[12,14,15] Most importantly, the best discrimination performance of an array

© 2023 Wiley-VCH GmbH

23669608, 2023, 3, Downloaded from https://onlinelibrary.wiley.com/doi/10.1002/smtd.202201352 by Korea Advanced Institute Of, Wiley Online Library on [20/03/2023]. See the Terms and Conditions (https://onlinelibrary.wiley.com/terms-and-conditions) on Wiley Online Library for rules of use; OA articles are governed by the applicable Creative Commons License

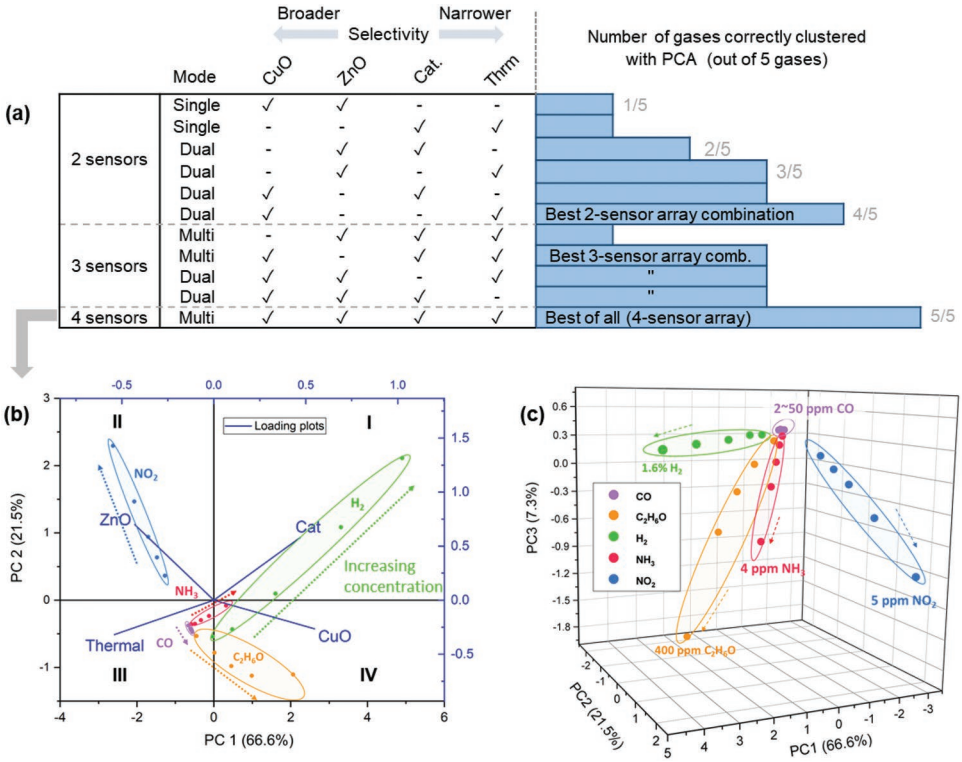


Figure 4. a) Results of combining all possible combinations of the four constituent sensors for sub arrays of 2 sensors, 3 sensors, and all four sensors; the bar chart on the right shows the number of non-overlapping clusters (with PCA) to identify the five gases. The array with four sensors performs best, clustering all of the gases tested. b,c) Projection of the 4D responses of the 4-sensors array for b) the first 2 principal components and c) the first 3 principal components.

is when all four sensors are utilized; this indicates that based on the properties of the target gases, the 4-sensor array (with all sensors) helps to discriminate their presence. On the other hand, by looking at the 2-sensor array combinations, we can see that single mode (or transduction) arrays do not perform well as they have a high degree of linearity (only one gas is clustered in this case); on the contrary, a dual-mode 2-sensor array, combining a CuO sensor (with broad selectivity) and the thermal conductivity sensor (narrower selectivity), shows very good results with 4 out of 5 gases clustered. The PCA plots for all combinations of 2-sensor arrays and 3-sensor arrays are shown in Figures S4,S5 (Supporting Information), respectively. The results in Figure 4 are consistent with previous studies where the combination of broadly selective and narrowly selective sensors shows superior discrimination performance, even though the number of sensors is lower than other combinations.[12,25] Specifically, similar to findings in previous research,[15,25] Figure 4a shows that, in some cases, a lower number of sensors (e.g., 2-sensor arrays) may yield higher discriminating performance, especially if there exist highly correlated sensors and/or sensors with lower sensitivity in arrays that combine higher numbers of sensors like the first case of the 3-element array where only one cluster is not overlapping with other gases (as shown in Figure S5, Supporting Information).

The PCA of the first 2 principal components and first 3 principal components of the 4-sensor array (the best array combination) are plotted in Figure 4b,c, respectively. As shown, PCA can cluster all five gases; however, as the concentration of each gas lowers, they converge to a common point and it may be harder to identify lower concentrations of gas. Even if the target gases may be classified well using a cluster classification algorithm (Linear Discriminant Analysis or Support Vector Machine) with a small number of sensors without reduction of the dimension using PCA, in the case of real-time gas identification, these algorithms may fail to classify the target gases due to limitations in decoding performances. For these reasons, CNNs are used in this research to help with real-time classification and regression.

2.5. Real-Time Classification and Regression with CNNs

CNNs have been traditionally used for image processing; they have also been applied to gas sensing applications.[32,33] However, in those studies, transient responses were not considered and thus real-time detection was not possible. In **Figure 5**a, we show the data processing strategy used herein to identify the target gases and quantify the concentrations of the gases in real-time using the four signals of the sensors. As shown in Figure 3a, there were transient regions for a quite long time because the responses of the sensors did not saturate immediately after the target gas injection. To perform real-time gas identification, it is essential to be able to classify the target gases and predict the concentration values of the gases even in the transient region. Therefore, in this work, a 5-second-sliding window was used to utilize the gradient information

© 2023 Wiley-VCH GmbH

23669608, 2023, 3, Downloaded from https://onlinelibrary.wiley.com/doi/10.1002/smtd.202201352 by Korea Advanced Institute Of, Wiley Online Library on [20/03/2023]. See the Terms and Conditions (https://onlinelibrary.wiley.com/terms-and-conditions) on Wiley Online Library for rules of use; OA articles are governed by the applicable Creative Commons License

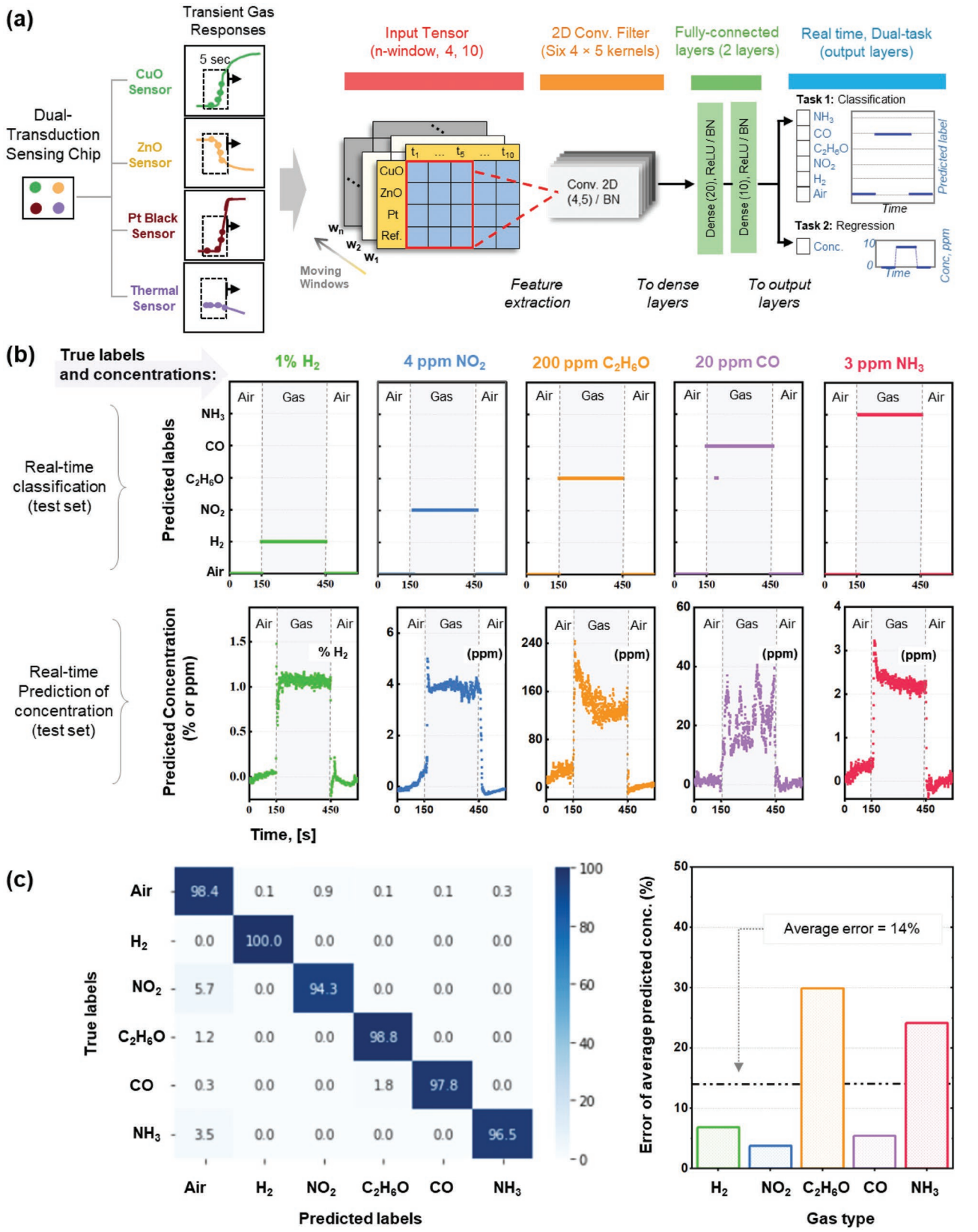


Figure 5. a) Data processing strategy to identify and quantify the concentrations of target gases in real-time using the four sensor signals. b) Real-time output (over time) of the classification task (top row) and regression task (bottom row). c) (left) Confusion matrix of the classification task showing high classification accuracy (>94%) for all gases, with an overall accuracy of 97.95%; (right) percent error of the regression task for each gas, showing an overall average error of 14 percent.

© 2023 Wiley-VCH GmbH

23669608, 2023, 3, Downloaded from https://onlinelibrary.wiley.com/doi/10.1002/smtd.202201352 by Korea Advanced Institute Of, Wiley Online Library on [20/03/2023]. See the Terms and Conditions (https://onlinelibrary.wiley.com/terms-and-conditions) on Wiley Online Library for rules of use; OA articles are governed by the applicable Creative Commons License

in the transient region, and the network structure was similarly designed to the real-time classification and regression algorithms previously published using a sliding window and CNNs.[6] In this work, a 5-second-sliding window was used to record the transient responses of all four sensors and the input data to the algorithm was built in the form of a tensor; the transient responses were sampled, simultaneously, at a rate of 2 Hz. For the gas identification, one-hot encoding and normalization were used to provide the algorithm with the true labels for the gas types and concentrations, respectively. In the gas tests, the gas concentration ranges were different depending on the target gas. If the concentration values of some specific gases are larger than those of other gases, there is a concern that the weight for predicting the specific gas concentration values can be greater than those of other gases in the network. Therefore, to prevent the CNNs from being biased against the specific gases in predicting the gas concentration due to the different concentration ranges of the target gases, the maximum gas concentration value used in the learning network for each target gas was normalized to 10 for the regression task. The preprocessed sensor signals were put into a 4×10 tensor, where every 0.5 s a new window was formed. The (n, 4, 10) windows were filtered by a 2D convolutional layer of size 4×5 every 2.5 s, that is, to extract features in the tensor built; this layer was followed by a batched normalization layer. The output of the filter was passed to two consecutive fully connected layers of sizes 20 and 10, respectively, both with Rectified Linear Unit activation layers and followed by batch normalization layers. Finally, as there are six gases (including air), the final output layer has six nodes for classification and an additional node was used for the regression task.

From the total transient responses presented in Figure 3a, we have divided 60% of the data for training, 20% for validation, and the remaining 20% for testing (Table S4, Supporting Information). As shown in Table S4 (Supporting Information), we aim to predict concentrations not previously seen during the training; these estimations represent more realistic scenarios encountered in normal operations. It is noteworthy to mention that these intermediate concentration estimations are more challenging to perform; such estimation has been previously reported in the literature with overall regression errors below 20% and a 100% classification accuracy;[10] a notable difference between the reference and this work is the fact that the classification and regression are done in real-time in this work. The output of the real-time classification task is shown in the top row of Figure 5b. As shown, the predicted labels for each gas, as a function of time, can be classified with only a few mislabels. In most cases, the misclassifications occur in the first few seconds after the gas is introduced or removed, as shown in the case of NO_2. The predicted gas concentration is shown in the bottom row of Figure 5b; the predicted concentration is close in value to the target. In certain cases, the relatively lower response of the sensors may result in fluctuations in the real-time prediction of the concentration (as in the case of CO predictions); a running average of the response can help obtain a more stable reading in real time. For example, as shown in Figure S6 (Supporting Information), a running average of 30 or 60 s can significantly reduce such fluctuations in the real-time reading of CO concentration. Finally, the real-time outputs shown in Figure 5b are summarized in Figure 5c. As shown from the confusion matrix, the overall classification accuracy is 97.95% while the average error of the mean predicted concentrations (versus the true concentrations) is 14%; these values are similar to those found in recent literature, with the added advantage of being done in real-time in this work.[6,10,21]

As expressed in references,[12,16] a one-size-fits-all array that can classify all possible gases does not exist because of the complex nature of chemical sensing. Thus, gas sensor arrays are designed to meet the sensing performance requirements set forth, which commonly include low-power and accurate detection. With this in mind, **Table 1** shows how our constructed array compares with other miniaturized gas sensor arrays based on the relevant performance and fabrication parameters; an extended form of this table is shown in Table S5 (Supporting Information), comparing other relevant dev ices.[6,8–11,20,21,27,34,35,36] As shown in these tables, chemiresistive-type sensors are widely used for multi-transduction arrays. This is because they provide high sensitivity and broad selectivity ranges that are advantageous for gas sensing. The surveyed multi-transduction arrays, in general, use a smaller number of sensors and a comparable number of gases are detected. The array in this work consumes much less total power than the other devices surveyed; we attribute this to the MEMS platform used and the local integration techniques. It is noteworthy to mention that in many cases, the total power consumption of multi-transduction arrays is not specified, and often complex, specialized circuity is utilized. The devices in Table 1 (and Table S5, Supporting Information) use supervised and non-supervised machine learning techniques for the classification and regression of the target gases. The device in this work provides comparable results for the classification (97.95% accuracy) and regression (14% average absolute error) as those in the references. Additionally, our device estimates concentrations not previously seen during the training (as done in the reference),[10] which is thought to represent better real-case scenarios. Another advantageous aspect of this work is that the detection for gas sensing is done in real-time.[6] Similar to most references surveyed, this work utilizes scalable techniques, which may allow for more compact or lower power operations. In summary, the device shown in this work shows comparable or superior performance for most parameters shown in Table 1. In this way, the research presented here is expected to contribute to one of the greatest challenges in the gas-sensing field: simultaneously achieving high selectivity, accuracy, and sensitivity at low-power operations with favorable response times.

The rational use of nanomaterials and advanced machine learning algorithms (and related technologies) have contributed to the advancement of other gas sensing-related applications, for example, from VOC detection[37] to breath analysis for disease diagnosis.[38] Similarly, the concept of a multi-transduction gas sensor chip, such as that presented in this work, can be very powerful for broader gas sensing applications. Concretely, by using the properties-specific responses of the constituent sensors and a machine learning algorithm, it may be possible to build a system that displays the properties of the gas being tested, rather than the name of the gas itself. For example, the array can output if the gas being detected is reducing or

© 2023 Wiley-VCH GmbH

23669608, 2023, 3, Downloaded from https://onlinelibrary.wiley.com/doi/10.1002/smtd.202201352 by Korea Advanced Institute Of, Wiley Online Library on [20/03/2023]. See the Terms and Conditions (https://onlinelibrary.wiley.com/terms-and-conditions) on Wiley Online Library for rules of use; OA articles are governed by the applicable Creative Commons License

Table 1. Comparison of miniaturized chemiresistive and multi-transduction arrays.

Ref.	Sensor type [a]			Sensors and gases tested			Data processing and performance results					Scalable integration method?[c]
	CR	CC/TC	GM	No. of sensors	No. of gases	Total power	Analysis method [b]	Classification (accuracy)	Regression [% error, MAE]	Untrained concentration?	Real time?	
[10]	✓	–	–	8	5	340 mW	SVM	100%	14.3%	✓	–	✓ CVD + Au seeds
[6]	✓	–	–	8	6	88 mW	CNN	98.1%	10.15%	–	✓	✓ GLAD + lithography
[21]	✓	–	✓	2	4	N/R	ΔI versus Δf_s	–	±5 – 20%	–	–	✓ PMMA tr. + E-beam
[30]	✓	✓	–	2	1	73 mW	–	–	–	–	–	**X** Drop casting
This work	✓	✓	–	4	5	28 mW	CNN	97.95%	14%	✓	✓	✓ Local hydrothermal + electrodeposition

[a]CR = Chemiresistive, CC = Catalytic Combustion, TC = Thermal Conductivity, GM = Gravimetric;; [b]SVM = Support Vector Machine, CNN = Convolutional Neural Network;; [c]CVD = Chemical Vapor Deposition, GLAD = Glancing Angle Deposition, PMMA tr. = Polymethyl methacrylate- supported transfer.

oxidizing, of higher or lower thermal conductivity than the air, combustible or noncombustible, etc. For this, a multi-label machine learning algorithm could be implemented, where the different gas properties are the output labels of the algorithm; this is a subject of our future work. By building and consulting databases of gas properties,[34] this approach can be very beneficial, as it may help to identify the nature of a gas that the array and algorithm have not seen before (i.e., an untrained sample), thus, broadening the scope of gases that the gas sensor array can detect while preserving the overall good performance reported herein.

3. Conclusion

In conclusion, we have developed a multi-transduction, low-power gas sensing chip for the sensing of flammable and toxic gases (H_2, NO_2, C_2H_6O, CO, and NH_3) at their risk-relevant concentrations, and also, with the aid of a machine learning algorithm, we could classify and quantify the target gases in real-time (classification accuracy of 97.95% and average error of the predicted concentration of 14%). The fabricated array, consisting of two calorimetric sensors (catalytic combustion and thermal conductivity) and two chemiresistive sensors (N-type and P-type), helps address a core issue in gas sensing, that is, achieving high selectivity/accuracy while operating at low power (7 mW per device). The attained high, real-time accuracy can be attributed to the orthogonal responses of the different sensors, according to the respective properties of each gas, and the utilized machine learning strategy. Meanwhile, the low power can be attributed to the low-power MEMS platform and the employed local integration synthesis techniques (electrodeposition and local hydrothermal synthesis), which allow for the integration in a small area (9 µm × 110 µm per individual sensor). This type of multi-transduction sensor chip with low-power operation shows great promise for portable, fast, and accurate detection of toxic and flammable gases. Moreover, a similar machine learning algorithm, but with multi-label output, could, in the future, help detect the properties of the gas being sensed (e.g., flammable/nonflammable, reducing/oxidizing, high/low thermal conductivity, etc.), which can help to identify the presence of a previously untrained gas.

4. Experimental Section

MEMS Platform Fabrication: The fabrication of the MEMS platform onto which all sensors are fabricated (Figure 1a) is described in detail elsewhere;[17] In summary, standard photolithographic techniques were followed with XeF_2 etching used to release the suspended microheaters. In this work, the top Au electrodes were modified from previous work,[17] that is, to have electrodes for chemiresistive and calorimetric devices on the same chip (as shown in Figure 2a).

Temperature Calibration of Microheater: The operating temperature of each sensor at 7 mW was estimated. For this, as shown in Figure S3 (Supporting Information), a tube furnace, a data logger, and a source meter were used. Uniform temperature changes in the tube furnace (up to 300 °C) were related to resistance changes in the microheater. It was compensated for the fact that only the microheater area was heated (and not the whole chip). Last, when the microheater acts as an RTD, for the catalytic and thermal conductivity sensors, it was useful to know quantitatively what temperature changes occur in the heater as a result of cooling or combustion; the obtained data and detailed procedure are shown in Figure S3 (Supporting Information).

Gas Sensing Measurements: The gas setup consisted of a stainless-steel chamber in which the chip was connected with pre-positioned electrodes and the gas was flown at a constant flow rate of 500 sccm using a mass flow controller. The detailed setup was explained in the previous work.[17] Here, an external dual output DC power supply (Agilent E3646A) was used to power the microheaters of the chemiresistive devices while two dual channel source meters (Keithley 2602B) measured the resistance changes of ZnO, CuO, and the RTDs (for the catalytic combustion sensor and the thermal conductivity sensor). The responses for the chemiresistive devices are defined as R_g/R_a, where R_g is the resistance of the ZnO or CuO sensor in the presence of gas and R_a is their resistance in the air. The response of the calorimetric sensors is expressed as $(R_g - R_a)/R_a$ (%), as in references,[17,18] where R_g and R_a are the resistances of the RTD (i.e., microheater) of the catalytic or thermal conductivity sensor in the target gas and in the air, respectively.

Signal Processing: The response of each sensor was analyzed with the PCA for clustering and with a supervised machine learning technique previously reported,[6] which utilized CNNs and a sliding window for real-time classification and regression. The OriginPro 2022 software was utilized for PCA and TensorFlow (version 2.7.0) was used for the supervised machine learning.

Supporting Information

Supporting Information is available from the Wiley Online Library or from the author.

© 2023 Wiley-VCH GmbH

23669608, 2023, 3, Downloaded from https://onlinelibrary.wiley.com/doi/10.1002/smtd.202201352 by Korea Advanced Institute Of, Wiley Online Library on [20/03/2023]. See the Terms and Conditions (https://onlinelibrary.wiley.com/terms-and-conditions) on Wiley Online Library for rules of use; OA articles are governed by the applicable Creative Commons License

Acknowledgements

D.V.D.O.H. and M.K. contributed equally to this work. This work was supported by the Development of Management Technology for HNS Accident (D11502815H480000140 2015034016), funded by the Ministry of Oceans and Fisheries, Korea. This work was also supported by the National Research Foundation of Korea (NRF) grants funded by the Korean government (MSIT) (No. 2021R1A2C300874212 and 2021M3H4A4079271).

Conflict of Interest

The authors declare no conflict of interest.

Data Availability Statement

Research data are not shared.

Keywords

calorimetric-type gas sensors, deep learning, MEMS, multi-transduction gas sensor arrays, nanomaterials, resistive-type gas sensors, toxic and flammable gases

Received: October 18, 2022
Revised: December 20, 2022
Published online: January 24, 2023

[1] S. Y. Park, Y. Kim, T. Kim, T. H. Eom, S. Y. Kim, H. W. Jang, *InfoMat* **2019**, *1*, 289.
[2] S.-J. Kim, S.-J. Choi, J.-S. Jang, H.-J. Cho, I.-D. Kim, *Acc. Chem. Res.* **2017**, *50*, 1587.
[3] K. Kang, D. Yang, J. Park, S. Kim, I. Cho, H.-H. Yang, M. Cho, S. Mousavi, K. H. Choi, I. Park, *Sens. Actuators, B* **2017**, *250*, 574.
[4] I. Choi, K. Kang, D. Yang, J. Yun, I. Park, *ACS Appl. Mater. Interfaces* **2017**, *9*, 27111.
[5] Q. Zhou, A. Sussman, J. Chang, J. Dong, A. Zettl, W. Mickelson, *Sens. Actuators, A* **2015**, *223*, 67.
[6] M. Kang, I. Cho, J. Park, J. Jeon, K. Lee, B. Lee, D. Del Orbe Henriquez, K. Yoon, I. Park, *ACS Sens.* **2022**, *7*, 430.
[7] D. Yang, K. Kang, D. Kim, Z. Li, I. Park, *Sci. Rep.* **2015**, *5*, 1.
[8] N. J. Pineau, J. F. Kompalla, A. T. Güntner, S. E. Pratsinis, *Microchim. Acta* **2018**, *185*, 563.
[9] D. S. Lee, S. W. Ban, M. Lee, D. D. Lee, *IEEE Sens. J.* **2005**, *5*, 530.
[10] N. X. Thai, M. Tonezzer, L. Masera, H. Nguyen, N. V. Duy, N. D. Hoa, *Anal. Chim. Acta* **2020**, *1124*, 85.
[11] A. T. Güntner, V. Koren, K. Chikkadi, M. Righettoni, S. E. Pratsinis, *ACS Sens.* **2016**, *1*, 528.
[12] A. Hierlemann, R. Gutierrez-Osuna, *Chem. Rev.* **2008**, *108*, 563.
[13] H. Ulmer, J. Mitrovics, U. Weimar, W. Göpel, *Sens. Actuators, B* **2000**, *65*, 79.
[14] M. Holmberg, F. Winquist, I. Lundström, J. W. Gardner, E. L. Hines, *Sens. Actuators, B* **1995**, *27*, 246.
[15] M. Pardo, L. G. Kwong, G. Sberveglieri, K. Brubaker, J. F. Schneider, W. R. Penrose, J. R. Stetter, *Sens. Actuators, B* **2005**, *106*, 136.
[16] F. Röck, N. Barsan, U. Weimar, *Chem. Rev.* **2008**, *108*, 705.
[17] D. V. Del Orbe, H. Yang, I. Cho, J. Park, J. Choi, S. Han, S. W. Han, I. Park, *Sens. Actuators, B* **2021**, *329*, 129129.
[18] A. Harley-Trochimczyk, J. Chang, Q. Zhou, J. Dong, T. Pham, M. A. Worsley, R. Maboudian, A. Zettl, W. Mickelson, *Sens. Actuators, B* **2015**, *206*, 399.
[19] A. Mahdavifar, R. Aguilar, Z. Peng, P. J. Hesketh, M. Findlay, J. R. Stetter, G. W. Hunter, *J. Electrochem. Soc.* **2014**, *161*, B55.
[20] F. Gao, W. Xuan, A. Bermak, F. Boussaid, C.-Y. Tsui, J. Luo, *Sens. Actuators, B* **2019**, *278*, 21.
[21] Y. Chen, H. Zhang, Z. Feng, H. Zhang, R. Zhang, Y. Yu, J. Tao, H. Zhao, W. Guo, W. Pang, X. Duan, J. Liu, D. Zhang, *ACS Appl. Mater. Interfaces* **2016**, *8*, 21742.
[22] Y. Li, C. Vancura, D. Barrettino, M. Graf, C. Hagleitner, A. Kummer, M. Zimmermann, K.-U. Kirstein, A. Hierlemann, *Sens. Actuators, B* **2007**, *126*, 431.
[23] H. Li, X. Mu, Y. Yang, A. J. Mason, *IEEE Sens. J.* **2014**, *14*, 3391.
[24] K. Kang, J. Park, B. Kim, K. Na, I. Cho, J. Rho, D. Yang, J.-Y. Lee, I. Park, *ACS Appl. Mater. Interfaces* **2020**, *12*, 39024.
[25] T. K. Alkasab, J. White, J. S. Kauer, *Chem. Senses* **2002**, *27*, 261.
[26] J. B. Miller, *IEEE Sens. J.* **2001**, *1*, 88.
[27] H. W. Shin, C. Lloyd, J. W. Gardner, *Transducers 97, Int. Conf. Solid-State Sens. Actuators* **1997**, *2*, 935.
[28] A. M. Feltham, S. Michael, *Chem. Rev.* **1971**, *71*, 177.
[29] C. R. K. Rao, D. C. Trivedi, *Coord. Chem. Rev.* **2005**, *249*, 613.
[30] D. Yang, H. Kim, S. H. Ko, A. P. Pisano, Z. Li, I. Park, *Adv. Mater.* **2015**, *27*, 1207.
[31] U. Hoefer, J. Frank, M. Fleischer, *Sens. Actuators, B* **2001**, *78*, 6.
[32] I. Essiet, Y. Sun, Z. Wang, *Procedia Manuf.* **2019**, *35*, 629.
[33] G. Wei, G. Li, J. Zhao, A. He, *Sensors* **2019**, *19*, 217.
[34] L. Wang, J. S. Swensen, *Sens. Actuators, B* **2012**, *174*, 366.
[35] M. Tonezzer, *Sens. Actuators, B* **2019**, *288*, 53.
[36] S. Acharyya, B. Jana, S. Nag, G. Saha, P. K. Guha, *Sens. Actuators, B* **2020**, *321*, 128484.
[37] B. Wang, J. C. Cancilla, J. S. Torrecilla, H. Haick, *Nano Lett.* **2014**, *14*, 933.
[38] N. Shehada, J. C. Cancilla, J. S. Torrecilla, E. S. Pariente, G. Brönstrup, S. Christiansen, D. W. Johnson, M. Leja, M. P. Davies, O. Liran, N. Peled, H. Haick, *ACS Nano* **2016**, *10*, 7047.

© 2023 Wiley-VCH GmbH

23669608, 2023, 3, Downloaded from https://onlinelibrary.wiley.com/doi/10.1002/smtd.202201352 by Korea Advanced Institute Of, Wiley Online Library on [20/03/2023]. See the Terms and Conditions (https://onlinelibrary.wiley.com/terms-and-conditions) on Wiley Online Library for rules of use; OA articles are governed by the applicable Creative Commons License